

Solution blow-spun polyacrylonitrile–polyamide thin-film nanofibrous composite membrane for the removal of fermentation inhibitors

Glebert C. Dadol, Leonard D. Tijing, Ramelito C. Agapay, Camila Flor Y. Lobarbio & Noel Peter B. Tan

To cite this article: Glebert C. Dadol, Leonard D. Tijing, Ramelito C. Agapay, Camila Flor Y. Lobarbio & Noel Peter B. Tan (2024) Solution blow-spun polyacrylonitrile–polyamide thin-film nanofibrous composite membrane for the removal of fermentation inhibitors, *Nanocomposites*, 10:1, 351-362, DOI: [10.1080/20550324.2024.2399978](https://doi.org/10.1080/20550324.2024.2399978)

To link to this article: <https://doi.org/10.1080/20550324.2024.2399978>



© 2024 The Author(s). Published by Informa UK Limited, trading as Taylor & Francis Group.



Published online: 11 Sep 2024.



Submit your article to this journal [↗](#)



Article views: 262




View related articles [↗](#)



View Crossmark data [↗](#)

Solution blow-spun polyacrylonitrile–polyamide thin-film nanofibrous composite membrane for the removal of fermentation inhibitors

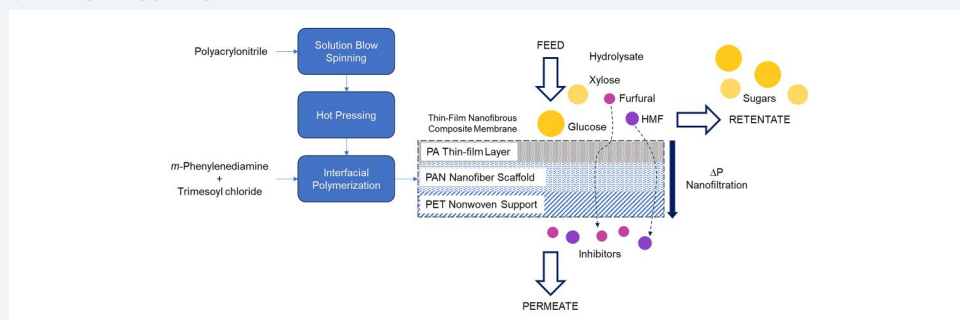
Glebert C. Dadol^a, Leonard D. Tijing^b, Ramelito C. Agapay^a, Camila Flor Y. Lobarbio^a and Noel Peter B. Tan^{c,d} 

^aDepartment of Chemical Engineering, School of Engineering, University of San Carlos, Cebu City, Philippines; ^bCentre for Technology in Water and Wastewater (CTWW), School of Civil and Environmental Engineering, University of Technology, Sydney (UTS), Broadway, New South Wales, Australia; ^cDepartment of Chemical Engineering, College of Technology, University of San Agustin, Iloilo City, Philippines; ^dCenter for Advanced New Materials, Engineering, and Emerging Technologies (CANMEET), University of San Agustin, Iloilo City, Philippines

ABSTRACT

This study aims to develop a thin-film nanofibrous composite (TFNC) membrane for removing fermentation inhibitors from a hydrolysate solution. Such membrane was fabricated via interfacial polymerization of a polyamide thin-film layer on top of a solution blow-spun polyacrylonitrile nanofiber scaffold. The effects of pH (3.29, 4.29, 8.26) and pressure (4, 6.67, 9.33, 12 bar) on the membrane's performance were investigated. The TFNC membrane had a high pure water permeability of 21.06 L/m²-h-bar and was able to deliver satisfactory rejection coefficients at pH 3.29 and pressure of 4 bar (glucose – 91.84%, xylose – 86.06%, hydroxymethylfurfural – 20.52%, furfural – 21.32%). Different pH settings resulted in similar permeate fluxes, but increasing the pH from acidic to basic reduced the rejection coefficients due to electrostatic repulsion. Increasing the pressure increased the permeate flux but decreased the rejection coefficients. The developed membrane showed remarkable permeability and effectively removed inhibitors, useful in biorefineries.

GRAPHICAL ABSTRACT



ARTICLE HISTORY

Received 29 April 2024
Accepted 29 August 2024

KEYWORDS



Thin-film nanofibrous composite membrane; solution blown spinning; polyacrylonitrile nanofibers; interfacial polymerization; hydrolysate detoxification; fermentation inhibitors; nanofiltration; reverse osmosis

1. Introduction

The world's pressing concerns include energy security, greenhouse gas emissions, and the depletion of fossil fuel reserves [1]. Bioethanol is an alternative and eco-friendly fuel in high demand. In the Philippines, bioethanol production is limited by insufficient feedstock and production capacity. Lignocellulosic materials from waste products can be used as feedstocks, and sugarcane bagasse alone can supply 1430 million liters of ethanol annually [2–4]. Lignocellulosic materials can be broken down into simpler sugars, e.g. glucose and xylose, through acid hydrolysis. This step also produces

hydroxymethylfurfural (HMF), furfural, and some organic acids, which can inhibit fermentation. Detoxification of hydrolysate to remove inhibitor compounds is crucial to boosting ethanol production. Membrane filtration is a promising detoxification process, capable of high inhibitor concentration reduction, having a modular configuration, not involving harmful chemicals, and capable of concentrating the sugars [5–7].

Conventionally, membranes for detoxication are Thin-Film Composite (TFC) membranes made up of a thin-film top layer, a porous middle layer, and a bottom support layer. The top layer, usually

CONTACT Noel Peter B. Tan  dtan@usa.edu.ph  Department of Chemical Engineering, College of Technology, University of San Agustin, Iloilo City, Philippines.

© 2024 The Author(s). Published by Informa UK Limited, trading as Taylor & Francis Group.

This is an Open Access article distributed under the terms of the Creative Commons Attribution-NonCommercial License (<http://creativecommons.org/licenses/by-nc/4.0/>), which permits unrestricted non-commercial use, distribution, and reproduction in any medium, provided the original work is properly cited. The terms on which this article has been published allow the posting of the Accepted Manuscript in a repository by the author(s) or with their consent.

polyamide (PA), is produced on the surface of the porous middle layer through interfacial polymerization (IP) by reacting an aqueous solution of amine monomer and an organic solution of acyl chloride monomer [8]. The porous middle layer is usually fabricated through phase inversion, producing asymmetric membranes with a dense top layer and a porous sub-layer. This structure creates discontinuities in the pores, resulting in closed and dead-end pores, which can lower the permeate flux of the membrane [9,10].

An alternative to the asymmetric membrane is a nanofibrous scaffold. The resulting membrane is called a Thin-Film Nanofibrous Composite (TFNC) membrane and has been shown to provide higher permeabilities at similar selectivity with TFC membranes. The high porosity and 'directed water channel' structures in TFNC membranes result in lower transport resistance and higher permeate flux [11]. As a result, these TFNC membranes have been increasingly explored for membrane-based processes such as nanofiltration [12], forward osmosis [13], membrane distillation [14], and others [15].

Solution blow spinning (SBS) is a promising nanofiber fabrication technology having high productivity without the reliance on high voltages and conductive polymers, unlike electrospinning. In SBS, the polymer solution is extruded through a nozzle and stretched into ultrafine fibers using pressurized air. The fibers dry up and collected on a substrate [16]. In one study, a TFNC membrane was fabricated with the middle layer made from a hot-pressed solution blow-spun polyacrylonitrile nanofiber scaffold. The pure water flux of the membrane was 13.1 L/m²-h at 4 bars with a salt (NaCl) rejection of 81.3% [17]. To our knowledge, such study is the first to use SBS to produce a nanofiber scaffold for a TFNC membrane. However, its applications were not explored aside from removing salts.

This study aims to develop, for the first time, a TFNC membrane for detoxification with a nanofibrous scaffold fabricated through SBS.

2. Experimental

2.1. Materials

Polyacrylonitrile (150 kDa MW, PAN), dimethyl formamide (99%, DMF), *m*-phenylenediamine (99%, MPD), trimesoyl chloride (98%, TMC), xylose ($\geq 99\%$), *n*-hexane (95%), phloroglucinol ($\geq 99\%$), and furfural (99%) were from Sigma-Aldrich. D-glucose anhydrous (analytical grade), acetic acid ($>80\%$), were from HiMedia Laboratories. Ethanol (99.5%) was from Chem-Supply. Acetonitrile (99.5%) was from Sharlau. Distilled water was from PSWRI.

2.2. Methods

2.2.1. Nanofiber scaffold fabrication

Solution blow-spun PAN nanofiber scaffold was fabricated as detailed in [18]. SBS was carried out by spinning 9% w/v PAN in DMF precursor solution using pressurized air (3 bar) in a specialized co-axial nozzle with ~ 40 cm working distance. The nanofiber scaffold was deposited on a polyester (PET) nonwoven substrate secured on a rotating collector and with the nozzle attached to a homogenizer moving side to side to ensure uniform deposition.

The PAN nanofiber scaffold was hot pressed using a hydraulic press (Model C, Carver, USA) with pressing conditions of 300 kPa and 100 °C for 5 min. The conditions were chosen based on the limitations of the equipment and results where the scaffolds did not incur physical damage.

2.2.2. Interfacial polymerization

PAN nanofiber scaffolds with dimensions of about 15 cm x 15 cm were fabricated into TFNC membranes. Before the Interfacial Polymerization (IP) process, the nanofiber scaffolds were soaked in 5% ethanol solution and washed with distilled water. Then, the nanofiber scaffold was clamped on a glass plate. The scaffold was soaked in 2% w/v MPD aqueous solution for 10 min. The MPD-saturated scaffold was taken out of the solution and the excess was removed by pressing the scaffold with a rubber roller. Afterward, a 0.1% TMC organic (*n*-hexane) solution was poured gently on the surface of the scaffold. The polymerization reaction was allowed to occur for 15 s before the excess TMC solution was washed with hexane. The membrane was cured inside the oven at 50 °C for 10 min [19]. The fabricated TFNC membranes were cut following the membrane cell template (active membrane area dimensions – 9.207 cm x 4.572 cm) and was washed with distilled water before soaking in distilled water for storage.

2.2.3. Filtration

A model hydrolysate solution was prepared with target compositions of 15 g/L glucose, 25 g/L xylose 0.3 g/L HMF, and 0.4 g/L furfural based on [20]. Initial pH of the hydrolysate was 6.18. The pH of the model solution was adjusted using HCl and NaOH. The pH of the solution was adjusted to target pH settings of 3, 4, and 8 which were chosen to simulate pH after acid hydrolysis, pH of the solution slightly above the isoelectric point of PA membranes, and a basic pH, respectively. Actual pH settings achieved were 3.29, 4.29, and 8.26.

The filtration setup was an assembled crossflow filtration system. It was composed of a multi-stage centrifugal pump (VSSM 1-17, Speroni, Italy), a

crossflow filtration membrane test cell (CF042D, Sterlitech, USA) with an effective membrane area of 42 cm² and a pressure control needle valve (6 A-V6LR-SS, Parker).

The prepared TFNC membrane was taken out of storage and placed inside the membrane cell. The operating pressures used in testing the membrane were 4, 6.67, 9.33, and 12 bars. The membrane was first subjected to compaction by operating the filtration system in total recirculation mode at four bars for at least 30 min with distilled water as feed. After compaction, the setup was allowed to reach a constant permeate flux by letting it run for another 30 min and taking flow rate measurements. Once the permeate flux was constant, final flow rate measurements (three trials) were taken and used for the permeate flux for that pressure. The pressure was raised to 6.67, 9.33, and 12 bar and the same procedure was followed for each pressure. The feed was replaced with the hydrolysate solution and the same procedure was followed. The hydrolysate pH was adjusted after testing all the pressures. At each pressure and pH setting of the feed, permeate samples were taken for analysis. Samples from the feed after every pH adjustment were taken to have an accurate feed composition.

Flow rate data from the filtration experiments were used to calculate the flux of pure water and the permeate. The permeate flux was determined using Equation (1).

$$J_i = \frac{\Delta V_i}{A_e t} \quad (1)$$

where J_i (L/m²-h or LMH) is the permeate flux of pure water or from the filtration of the model solution, ΔV_i (L) is the volume collected of the pure water permeate or the permeate from the model solution, A_e (m²) is the effective membrane area, and t (h) is the time elapsed after collecting the volume of the pure water or the permeate from the model solution.

The pure water permeability of the TFNC membrane was determined from the slope of the pure water flux vs pressure data.

2.3. Characterization and analysis

2.3.1. PAN nanofiber scaffold and TFNC membrane characterization

The thickness of the PAN nanofiber scaffold, and TFNC membranes were determined using a dial thickness gauge (Mitutoyo 7301, Japan). The porosity of the PAN nanofiber scaffolds and the TFNC membranes were determined through gravimetric method or from the proportion of the void volume to the total volume [17]. The porosity of the sample was determined using Equation (2)

$$\varepsilon = \frac{M_w - M_s}{l_s w_s t_s \rho_w} \quad (2)$$

where ε is the porosity, M_w (g) and M_s (g) are the weight of the wet and dry sample, respectively, l_s (cm), w_s (cm), and t_s (cm) are the length, width, and thickness of the sample, respectively, and ρ_w (g/cm³) is the density of water.

Fourier Transform Infrared (FTIR) spectra of the PAN nanofiber scaffold and TFNC membrane were obtained using Shimadzu IRAffinity-1S with MIRacle 10 single-reflection attenuated total reflection (ATR) method at 22 °C and acquired over 4600–600 cm⁻¹.

The morphologies of the PAN nanofiber scaffold and TFNC membrane were determined through Field Emission Scanning Electron Microscope (FESEM) imaging. A sample was sputter-coated with platinum. Imaging was done using a Dual Beam Helios Nanolab 600i with voltage of 2.00 kV and beam current of 86 pA. The pore size and average fiber diameter of the nanofiber scaffold were determined from the FESEM images using ImageJ software.

2.3.2. Model solution and permeate analysis

Glucose and xylose concentrations of the model solution and the permeate samples were determined using the dual-wavelength colorimetry method. The samples were diluted to 1:50, colored with a phloroglucinol solution (2 g in 110 mL glacial acetic acid, 10 mL ethanol, and 2 mL concentrated HCl), and heated in a water bath at 100 °C for 10 min. The samples were then cooled in an ice water bath for 5 min. Absorbance readings of the solution at 425 nm and 553 nm were taken using a spectrophotometer (UV-1900i, Shimadzu, Japan). The concentrations of the sugars were calculated as detailed in [21].

The concentrations of furfural and HMF in the model solution and permeate samples were determined using a High-Performance Liquid Chromatography (HPLC) instrument (Shimadzu, Japan) equipped with a C-18 reverse-phase column (ODS-3V Inertsil, Europe), a high-pressure pump (LC-10AT), an oven (CTO-10A), and a UV-Vis detector (SPD-10AV) was used. The mobile phase was a mixture of acetic acid, acetonitrile, and water with a volumetric ratio of 1:11:88. Samples were filtered using a syringe filter (PTFE 0.20 µm, Fisherbrand) and 20 µL of the filtered samples was injected into the HPLC system with a temperature of 30 °C and a constant elution flow rate of 1 mL/min. The absorbance was measured at 254 nm, and the concentrations of furfural and HMF were determined from a calibration curve using standard solutions.

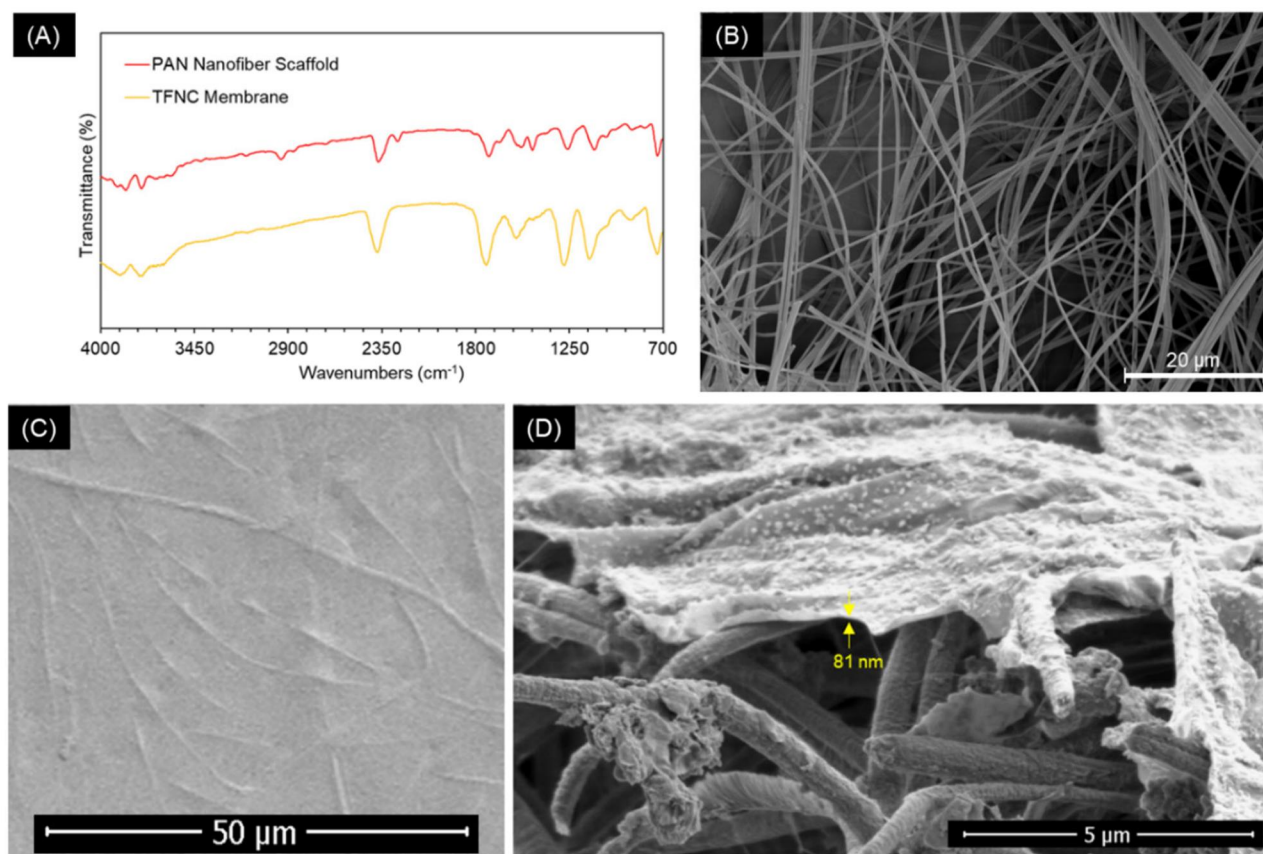


Figure 1. (A) FTIR spectra of the PAN nanofiber scaffold and TFNC membrane, FESEM images of the (B) nanofiber scaffold, (C) TFNC membrane, and (D) cross-sectional view of the TFNC membrane showing the measurement of the thickness of the PA layer.

The rejection coefficient of glucose, xylose, furfural, and HMF was determined using Equation (3).

$$R_i = \left(1 - \frac{C_{i,p}}{C_{i,f}} \right) \times 100 \quad (3)$$

where R_i (%) is the rejection coefficient of the solute, $C_{i,p}$ (g/L) is the concentration of the solute in the permeate, and $C_{i,f}$ (g/L) is the concentration of the solute in the feed.

The pore size of the TFNC membrane was determined from the rejection coefficient vs permeate flux data of glucose and xylose using the Spiegler and Kedem membrane transport (SKMT) model [22] and the steric-hindrance pore (SHP) model [23].

3. Results and discussion

3.1. Characterization of PAN nanofiber scaffolds and TFNC membranes

The nanofiber scaffold had a total thickness of $113.17 \pm 4.37 \mu\text{m}$ with a PAN layer measuring $12.67 \pm 5.44 \mu\text{m}$. Its porosity was $63.50 \pm 6.29\%$ with surface pore size and average fiber diameter of $1.75 \pm 1.50 \mu\text{m}$ and $565.20 \pm 243.70 \text{ nm}$, respectively. Compared to electrospun PAN nanofibers that have been used to fabricate TFC membranes, the scaffold

in this work was thinner, but had similar porosities and surface pore sizes [24–26]. The porosity of electrospun and solution blow-spun nanofibers were previously reported to be at least 70% and as high as 95% [27,28] and pore sizes in the range of 0.1–10 μm which make them good scaffolds for composite membranes [29,30]. The average fiber diameter of the PAN nanofibers in this study was considered to be on the high side since solution blow-spun nanofibers have average fiber diameters in the range of 50–700 nm [31,32]. TFNC membranes fabricated from nanofiber scaffolds with larger fiber sizes were found to result in larger membrane pore size, higher permeate flux and lower rejection [33].

Shown in Figure 1(A) is the FTIR spectra of the PAN nanofiber scaffold and TFNC membrane. The peak at 2400 cm^{-1} corresponds to $\text{C} \equiv \text{N}$ groups due to the presence of PAN, and the peak at 1540 cm^{-1} corresponds to N-H groups which confirms the presence of polyamide (PA) in the TFNC membrane [34,35]. Shown in Figure 1(B) is the FESEM image of the PAN nanofiber scaffold. The image shows typical solution blow-spun PAN nanofiber morphology with randomly overlapping and curly appearance [36]. Shown in Figure 1(C) is the FESEM image of the TFNC membrane. The figure shows the polyamide (PA) layer on top of the nanofibers. In

Figure 1(D), the cross-sectional image of the membrane is depicted. It shows the PA layer with a thickness of ~ 81 nm on the surface of the porous PAN nanofiber scaffold. This agrees with previously reported PA layer thickness of TFNC membranes of 50–120 nm [17,37,38].

3.2. Filtration performance

The pure water permeability of TFNC membrane was 21.06 ± 0.57 L/m²-h-bar (LMHB) which was superior to TFC membranes used for hydrolysate detoxification in previous works [7,39–42]. The commercial membrane NF270 which is a TFC membrane with a PA barrier layer commonly used for hydrolysate detoxification only delivered a pure water permeability of 16.51 LMHB as tested by a different study [39]. The high permeability of the TFNC membrane is due to the nanofibrous structure of the middle layer. The high porosity and interconnected pores of the nanofibers provide directed water nanochannels with low transport resistance resulting in higher permeability compared to conventional TFC membranes [11,43].

The hydrolysate permeability and hydrolysate permeate flux of the TFNC membrane at pH 3.29 and 4 bar were 23.92 ± 3.54 LMHB and 5.76 LMH, respectively. At the same conditions, the rejection coefficient of the membrane for glucose, xylose, HMF, and furfural were 91.84%, 86.08%, 20.52%, and 21.32%, respectively. As a membrane for detoxification, the performance is satisfactory since the rejection coefficient for the sugars are high and for the inhibitors are low.

In one study [7], they used NF90 and NF270 membranes for detoxification. Detoxification using NF90 of a model hydrolysate solution with pH 3 at 5 bar resulted in rejection coefficients for glucose, xylose, HMF, and furfural of $\sim 98\%$, $\sim 97\%$, $\sim 50\%$, and $\sim 20\%$, respectively. At the same conditions and for the same model solution, using NF270 membrane resulted in rejection coefficients for glucose, xylose, HMF, and furfural of $\sim 87\%$, $\sim 69\%$, $\sim 2\%$, and $\sim 1\%$, respectively. NF90 is better at filtering the sugars while NF270 allows more of the inhibitors to pass through since NF90 has a pore size of 0.73 nm [44] while NF270 has a pore size 0.84 nm [45]. The TFNC membrane in this work has a pore size in between the pore sizes of those membranes (based on glucose at pH 3.29) which is in agreement when comparing the rejection coefficient data.

Summarized in Table 1 are the filtration performance of the membranes used for the detoxification of hydrolysate solutions including this work. It can be seen that the TFNC membrane from this work has superior pure water permeability compared to

all other membranes. It also has high rejection coefficients for sugars. However, the rejection coefficient for the inhibitors are on the high side when compared to other studies with extremely low rejection coefficient for the inhibitors, although differences in hydrolysate concentration and process conditions can affect the rejection coefficient.

Compared to the work of [39], the performance of the TFNC in this work was somewhere in the middle of the performance of NF90 and NF270 membranes. Some membranes from other studies show higher rejection coefficients for sugars and lower rejection coefficient for the inhibitors. In comparison with [42], they were able to achieve higher rejection coefficients for the sugars which could be attributed to using higher pressures although the DK1812-34D membrane they used was able to keep the rejection for the inhibitors low. From [7], most of the membranes they tested had higher rejection coefficients for the sugars due to a higher operating pressure (up to 30 bar), but the rejection coefficients for the inhibitors were also quite high except for the NF- and NF245 membranes. From [6], both nanofiltration and RO membranes showed high rejection for the sugars, but the RO membranes also resulted in extremely high rejection for the inhibitors.

The membrane in this work shows promise as an alternative membrane used for detoxification with high permeability and decent rejection coefficient. There is also great potential in further improving its performance by employing modifications such as using graphene oxide, nanomaterials, and deep eutectic solvents [46].

3.3. Effect of pH

Shown in Figure 2(A) is the permeate flux at different model hydrolysate pH. It can be seen from the figure that the permeate flux is only slightly affected by the pH of the solution. There was no significant difference in the permeate flux in each of the pressure setting at all pH ($p > 0.05$). In one study [6], filtration of a model hydrolysate solution using commercial membranes (Desal 5-DK, RO98pHt, RO99) at 30 bar resulted in no changes to the permeate flux while varying the pH of the solution from 2 to 10. Most composite membranes with PA active layer have a pH resistance of 2–11 and as long as the membrane is intact and stable, the permeate flux should be unaffected by the pH of the solution [40,47].

Shown in Figure 2(B,C) are the rejection coefficients of the sugars and inhibitors, respectively, at different solution pH and pressure of 4 bar. It can be seen from the figures that the rejection

Table 1. Summary of membranes used for detoxification (including this work).

Membrane	Supplier	Pore diameter (nm)	Pure water permeability (LMHB)	Process conditions	Rejection coefficient (%) ^a	Hydrolysate composition	Reference
SBS PAN-PA TFNC	N/A	0.76 ^c	21.06	4–12 bar pH – 3.29, 4.29, 8.26 Ave temp 36 °C	<i>For pH 3.29:</i> Glucose – 92–95 Xylose – 86–90 Furfural – 21–26 HMF – 21–26	Glucose – 10.05–13.74 g/L Xylose – 22.14–25.8 g/L Furfural – 0.38–0.47 g/L HMF – 0.20–0.22 g/L	This work
NF90	Dow Filmtec	0.68 ^d	7.56	4–20 bar pH – 3, 5.5 Room temp	<i>For pH 5.5:</i> Glucose – 57–80 Xylose – 55–79 Furfural – 5–30 HMF – 6–25	Glucose – 2.3 g/L Xylose – 37.3 g/L Arabinose – 3.4 g/L Formic acid – 2.1 g/L Acetic acid – 13.7 g/L	[39]
NF270	Dow Filmtec	0.84 ^d	16.51		<i>For pH 5.5:</i> Glucose – 75–92 Xylose – 57–75 Furfural – 2–7 HMF – 3–8	Levulinic acid – 0.4 g/L HMF – 0.5 g/L Furfural – 3.6 g/L	
DK1812-34D	GE Osmonics	0.79 ^d	8.17	6–24 bar pH – 3, 5, 7, 9 25 °C	<i>For 20 bar pressure:</i> Glucose – 93–99 Xylose – 83–95 Furfural – 2–5 HMF – 10–14	Corn cob Hydrolysate (composition nr)	[42]
CPA2	Hydraunatics	nr	3.1	5–30 bar pH 3 20 °C	Glucose – 95–97 Xylose – 95–97 Furfural – 13–43 HMF – 42–79	Glucose – 10 g/L Xylose – 15 g/L Arabinose – 5 g/L Furfural – 0.5 g/L	[7]
CPA3	Hydraunatics	nr	2.6		Glucose – 97–99 Xylose – 95–98 Furfural – 12–40 HMF – 39–77	HMF – 1 g/L Acetic acid – 5 g/L Vanillin – 0.05 g/L	
ESPA2	Hydraunatics	nr	5.8		Glucose – 97–99 Xylose – 95–98 Furfural – 31–72 HMF – 74–95		
XLE	Dow Filmtec	nr	7.7		Glucose – 98–99 Xylose – 97–98 Furfural – 62–95 HMF – 90–100		
SG	GE Osmonics	nr	2.7		Glucose – 95–99 Xylose – 95–98 Furfural – 19–56 HMF – 53–86		
NF-	Dow Filmtec	nr	5.6		Glucose – 94–97 Xylose – 77–92 Furfural – 2–3 HMF – 3–15		
NF245	Dow Filmtec	nr	3.7		Glucose – 91–96 Xylose – 70–89 Furfural – 1–2 HMF – 2–14		
Desal-5 DK	GE Osmonics	0.8–0.9	7.8	20–45 bar pH – 2.5–10 25 °C	<i>For pH 6.43:</i> Glucose – 95–98 Xylose – 82–91 Furfural – (-1)-1 HMF – 1	Glucose – 4–20 g/L Xylose – 10–50 g/L HMF – 0.05–0.5 g/L Furfural – 2–10 g/L	[6]
Alfa Laval-NF	Alfa Laval	nr	10.08		<i>For pH 6.43:</i> Glucose – 95–98 Xylose – 81–84 Furfural – (-1)-1 HMF – 1		
RO98pHt	Alfa Laval	nr	3.15		<i>For pH 6.43:</i> Glucose – 99–100 Xylose – 96–98 Furfural – 73–86 HMF – 73–85		
RO99	Alfa Laval	nr	2.6		<i>For pH 6.43:</i> Glucose – 99–100 Xylose – 99 Furfural – 79–88 HMF – 79–88		

Notes: nr: not reported. ^aOnly values for glucose, xylose, furfural and HMF are shown here, ^bbased on xylose at pH 3.29, ^cbased on xylose with no pH change, and ^dbased on xylose at pH 3.

coefficients of the sugars and inhibitors decrease as the pH of the solution is increased. This trend is also observed for rejection coefficients at the other

pressures. Similar observations were made from previous studies using TFC membranes in the detoxification of hydrolysates [40,42].

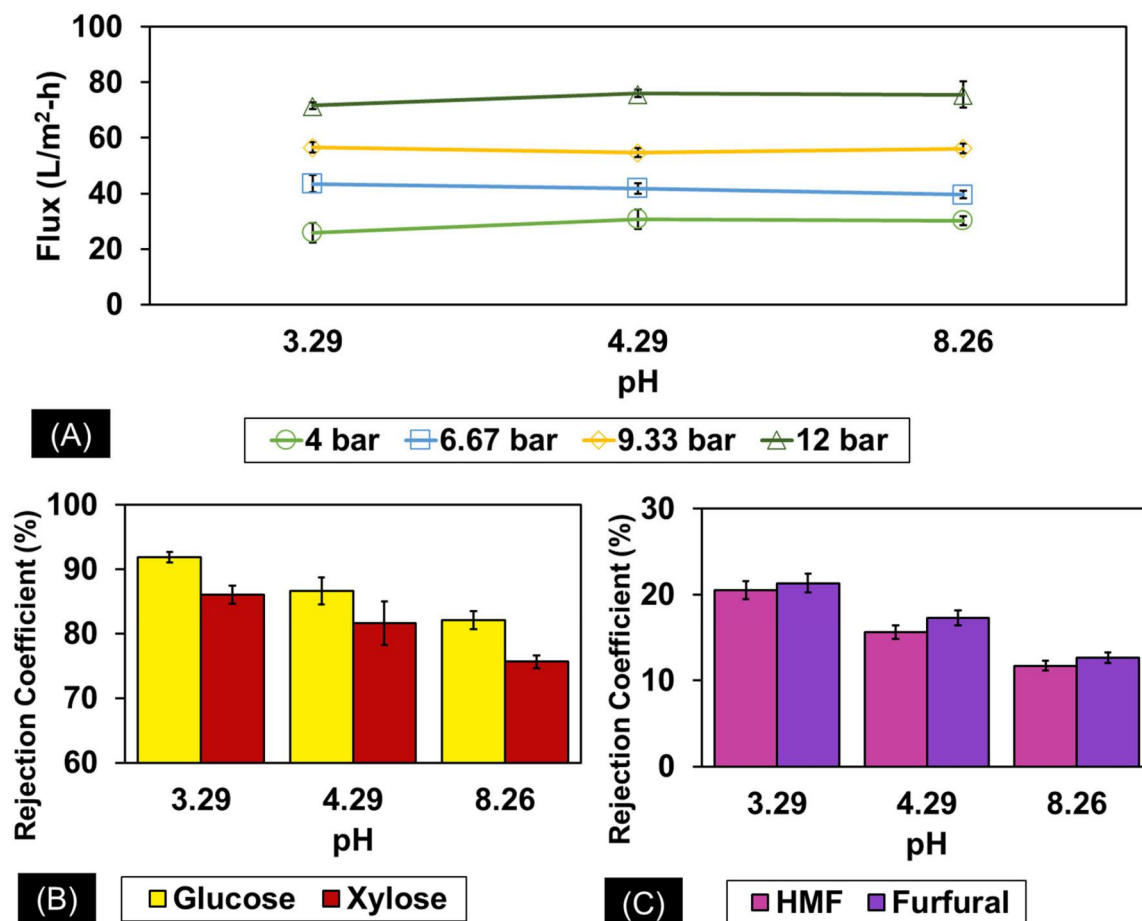


Figure 2. (A) Permeate flux (all pressures), and rejection coefficients of (B) sugars and (C) inhibitors (4 bar) using the TFNC membrane at different pH.

Table 2. Pore size of TFNC membrane determined from flux-rejection data and the Spiegler and Kedem membrane transport (SKMT) and steric-hindrance pore (SHP) models.

pH	Pore Size (nm)	
	Based on glucose	Based on xylose
3.29	0.8161	0.7581
4.29	0.8491	0.7968
8.26	0.8984	0.8590

Glucose, xylose, HMF and furfural have dissociation constants greater than 12 [40,41] which means that they are neutral at the pH settings selected for the model hydrolysate in this work. For uncharged solutes, the effect of pH on the filtration performance can be described by the intramembrane electrostatic repulsion. Membranes with PA active layer have been previously reported to have an isoelectric point of 3–4 [42,47–49]. In the filtration of solutions with pH at the isoelectric point, the membrane will have no effective charge. As the pH is increased, ionizable groups in the PA layer can dissociate and provide the pores of the membrane with negative charges [50,51]. The negative charges on the membrane pores will repel against each other resulting to an increase in the pore size.

Listed in Table 2 are the pore sizes of the TFNC membrane determined from the flux and rejection

data, and the SKMT-SHP model. The pore size based on the data for glucose are greater than that of xylose since the Stokes diameter of glucose (0.726 nm) is greater than of xylose (0.638 nm) [41]. Additionally, the pore sizes increase as the pH increases. The computed pore sizes are in agreement with reported pore sizes of TFC membranes used for hydrolysate detoxification which is around 0.7–0.9 nm based on xylose rejection and permeate flux data [6,39,40].

A schematic representation of the mechanism for the effect of pH on the rejection coefficient for the sugars and inhibitors is shown in Figure 3. In summary, increasing the pH of the hydrolysate solution results to electrostatic repulsion of the membrane pores which enlarges the pore size allowing more solutes to pass through the permeate side and ultimately, lowering the rejection coefficient. Since most hydrolysates have pH of around 3, proceeding with the detoxification without or minimal pH adjustment is practical to obtain high rejection coefficients for the sugars.

3.4. Effect of pressure

Shown in Figure 4(A) is the permeate flux of filtration of the model hydrolysate solution with pH 3.29

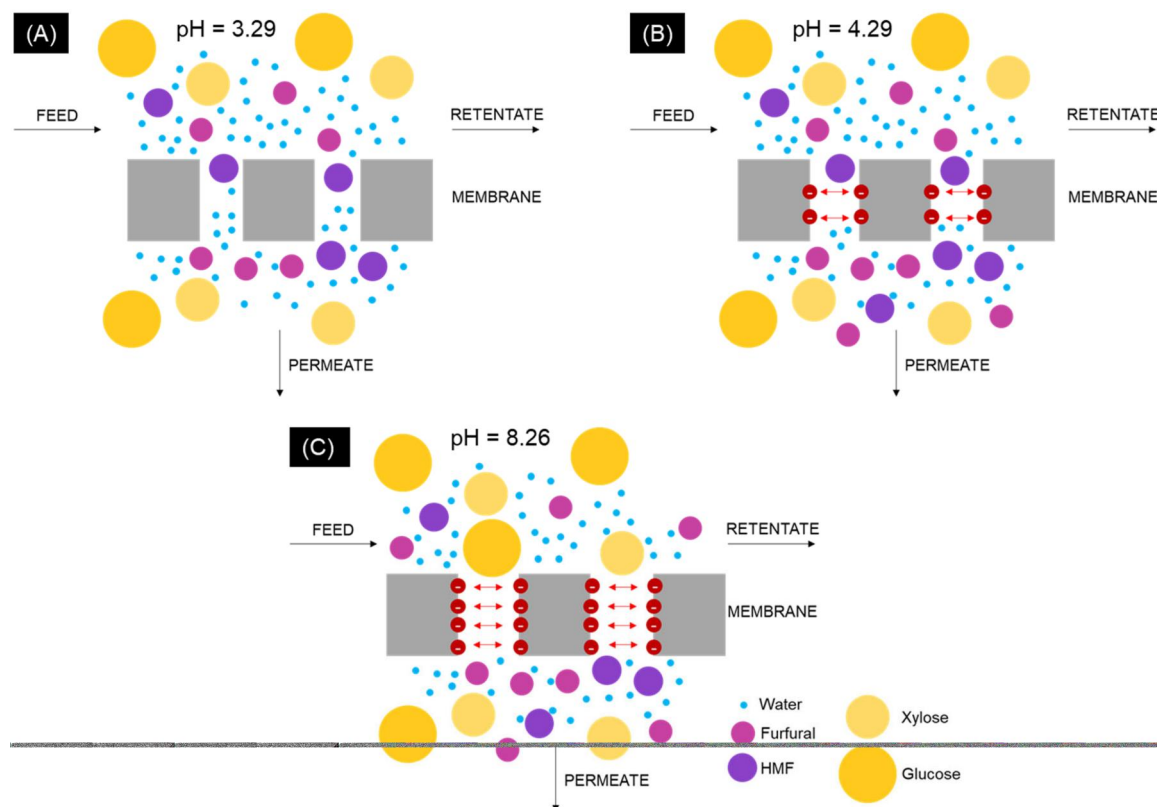


Figure 3. Schematic representation of the intramembrane electrostatic repulsion describing the decrease in the rejection coefficient with increasing pH: (A) pH 3.29, (B) pH 4.29, and (C) 8.26.

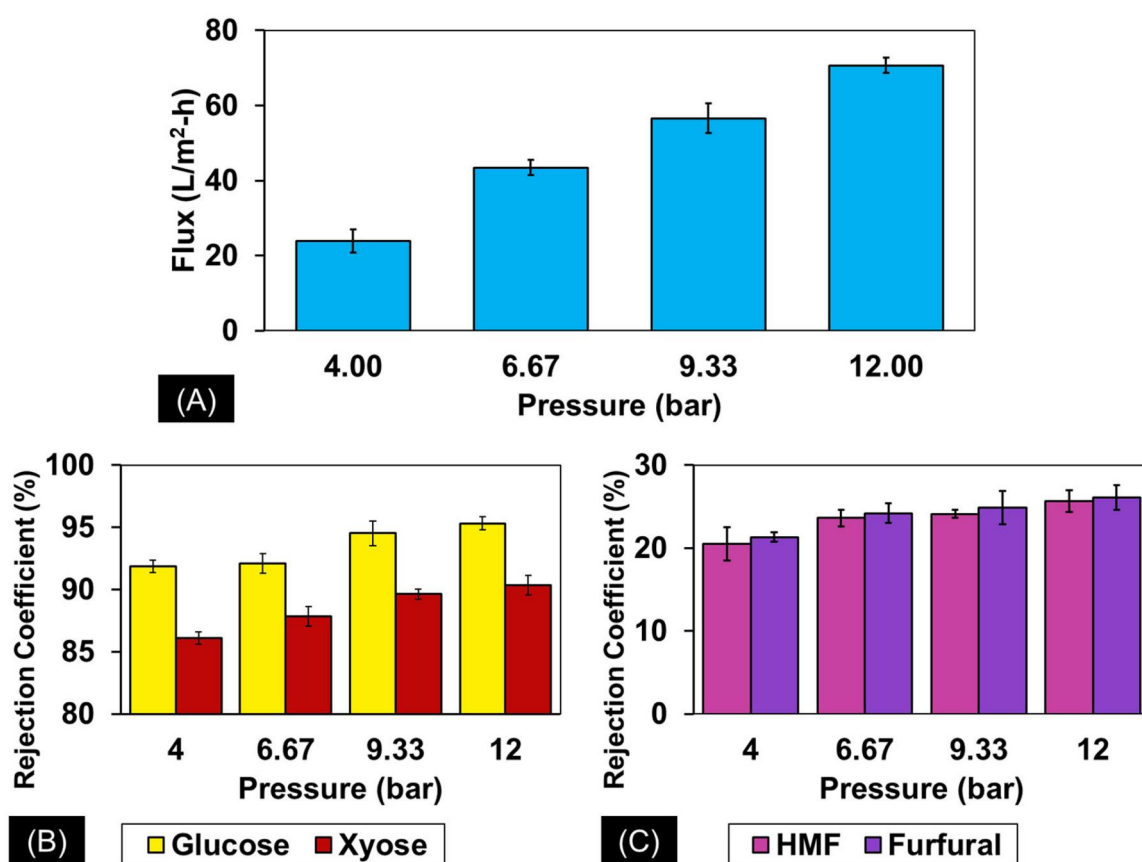


Figure 4. (A) Permeate flux, and rejection coefficients of (B) sugars and (C) inhibitors using the TFNC membrane at pH 3.29 and different pressures.

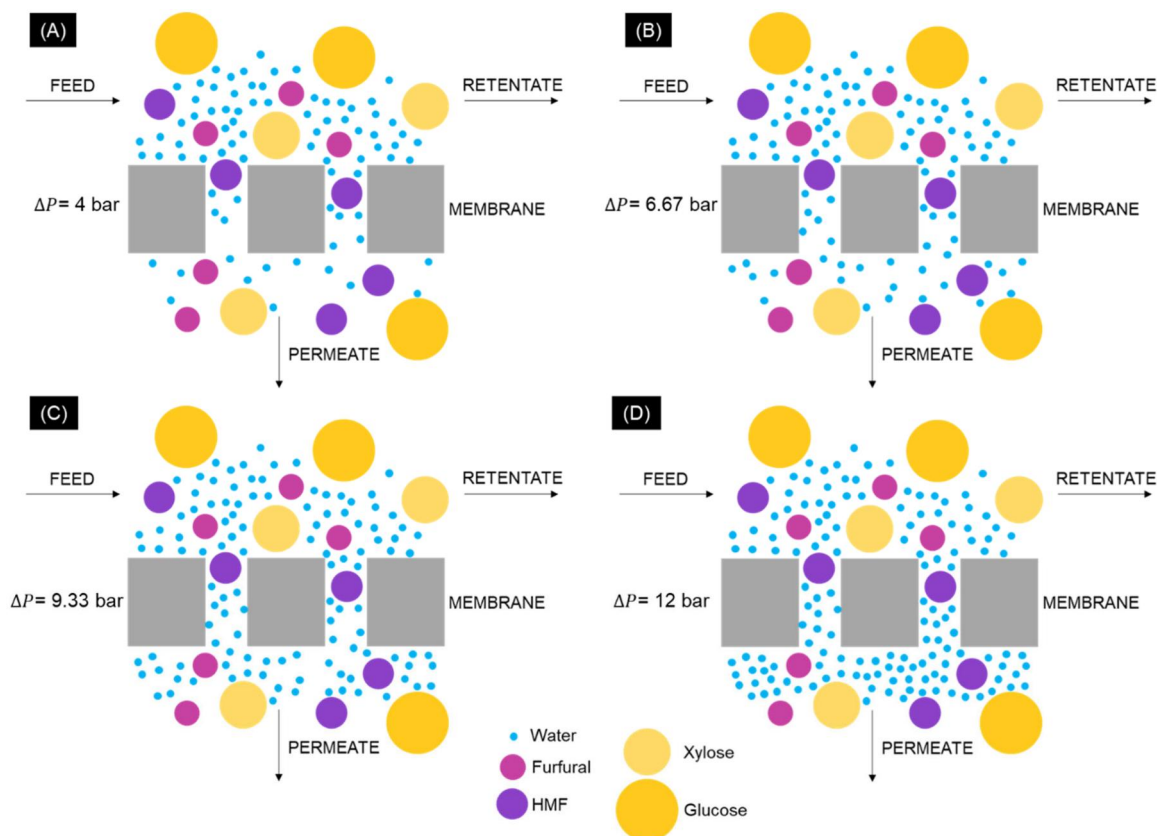


Figure 5. Schematic representation of the solution-diffusion mechanism describing the effect of pressure on the rejection coefficients at (A) 4, (B) 6.67, (C) 9.33, and (D) 12 bars.

at different pressures. Expectedly, the permeate flux increases as the pressure is increased in accordance with the results from other studies [6,7]. This trend is observed in the filtration of hydrolysate solutions at different pH settings as well. Filtration is a pressure-driven process and according to the Hagen-Poiseuille Law, the permeate flux increases directly with the applied pressure [52].

Shown in Figure 4(B,C) are the rejection coefficients of the sugars and inhibitors, respectively, at pH 3.29 and different pressures. It can be seen from the figures that the rejection coefficients for both sugars and inhibitors increase as the pressure is increased. This trend is also observed in the filtration of the hydrolysate solution with the other pH settings. In this work, the highest rejection coefficient for glucose and xylose were 95.32% and 90.35%, respectively, at 12 bars and solution pH of 3.29. At the same conditions, the rejection coefficient for the inhibitors were also highest for HMF and furfural at 25.63% and 26.08%, respectively.

In a different study [39], NF90 and NF270 membranes were used in the detoxification of a model hydrolysate solution based on extracted olive pomace and the filtration was operated with pressures of 4, 6, and 9 bar. The rejection coefficient all increased as the pressure was increased for glucose (58%–75%–80%), xylose (58%–75%–80%), HMF (6%–14%–25%), and furfural (4%–10%–30%).

A schematic representation of the mechanism for the effect of pressure on the rejection coefficient for the sugars and inhibitors is shown in Figure 5. When the pressure is increased during filtration, water diffuses more into the membrane and to the permeate side. This dilutes the solution on the permeate side resulting in a higher computed rejection coefficient [53]. Increasing the pressure increases the permeate flux and the rejection coefficient of the sugars. However, it also increases the rejection coefficient of the inhibitors which is unfavorable since the inhibitors must be removed to detoxify the hydrolysate. Therefore, the filtration has to be operated at the appropriate pressure to remove as much inhibitors and retain the sugars needed for fermentation.

4. Conclusion

The feasibility of using a solution blow spun PAN-PA composite nanofiltration membrane for the removal of fermentation inhibitors was investigated in terms of the effect of pH and pressure on the filtration performance for a sugarcane bagasse simulated hydrolysate. The TFNC membrane was able to deliver a high pure water permeability of 21.06 LMHB and achieve decent rejection coefficients for glucose (91.84%), xylose (86.08%), HMF (20.52%), and furfural (21.32%). Among the conditions used

in this study, a pH of 3.29 and pressure of 12 bars provided high permeate flux (>70 LMH) while still ensuring high rejection coefficients for the sugars (>80%) and low rejection coefficients for the inhibitors (<20%).

Acknowledgments

The authors would like to thank Norielle Marie B. Tornalejo of the Gregor Mendel Research Laboratories, University of San Agustin for the FTIR analysis.

Disclosure statement

No potential conflict of interest was reported by the author(s).

Funding

This work was funded by the Department of Science and Technology (DOST) Engineering Research and Development for Technology (ERDT) Scholarship.

Notes on contributors

Glebert C. Dadol Conceptualization, Methodology, Validation, Investigation, Writing – Original Draft, Visualization.

Leonard D. Tijing Writing – Review & Editing.

Ramelito C. Agapay Writing – Review & Editing.

Camila Flor Y. Lobarbio Writing – Review & Editing.

Noel Peter B. Tan Conceptualization, Writing – Review & Editing, Supervision, Project administration.

ORCID

Noel Peter B. Tan  <http://orcid.org/0000-0002-5424-9616>

References

- Halder P, Azad K, Shah S, et al. Prospects and technological advancement of cellulosic bioethanol ecofuel production. In: *Advances in eco-fuels for a sustainable environment*. Sawston, UK: Elsevier; 2019. doi: [10.1016/b978-0-08-102728-8.00008-5](https://doi.org/10.1016/b978-0-08-102728-8.00008-5).
- Department of Energy. Philippine energy plan 2016–2030. Philippines: Department of Energy; 2016.
- Mojica-Sevilla F. Biofuels annual. USA: USDA; 2021.
- Go AW, Tabañag IDF, Ju Y, et al. Sugarcane processing by-products for bioethanol production in the Philippines: a retrospective assessment from 2007 to 2017 and future challenges. *Biofuels*. 2020;13(5):567–577. doi: [10.1080/17597269.2020.1812999](https://doi.org/10.1080/17597269.2020.1812999).
- Qian X, Malmali M, Wickramasinghe SRR. Membranes for the removal of fermentation inhibitors from biofuel production. In: *Membrane technologies for biorefining*. Sawston, UK: Elsevier; 2016. p. 219–240. doi: [10.1016/B978-0-08-100451-7.00009-8](https://doi.org/10.1016/B978-0-08-100451-7.00009-8).
- Wang T, Meng Y, Qin Y, et al. Removal of furfural and HMF from monosaccharides by nanofiltration and reverse osmosis membranes. *J Energy Inst*. 2018; 91(3):473–480. doi: [10.1016/j.joei.2017.01.005](https://doi.org/10.1016/j.joei.2017.01.005).
- Nguyen N, Fargues C, Guiga W, et al. Assessing nanofiltration and reverse osmosis for the detoxification of lignocellulosic hydrolysates. *J Membr Sci*. 2015;487:40–50. doi: [10.1016/j.memsci.2015.03.072](https://doi.org/10.1016/j.memsci.2015.03.072).
- Brami MV, Oren Y, Linder C, et al. Nanofiltration properties of asymmetric membranes prepared by phase inversion of sulfonated nitro-polyphenylsulfone. *Polymer*. 2017;111:137–147. doi: [10.1016/j.polymer.2017.01.048](https://doi.org/10.1016/j.polymer.2017.01.048).
- Liu R, Xu X, Zhuang X, et al. Solution blowing of chitosan/PVA hydrogel nanofiber mats. *Carbohydr Polym*. 2014;101:1116–1121. doi: [10.1016/j.carbpol.2013.10.056](https://doi.org/10.1016/j.carbpol.2013.10.056).
- Yung L, Ma H, Wang X, et al. Fabrication of thin-film nanofibrous composite membranes by interfacial polymerization using ionic liquids as additives. *J Membr Sci*. 2010;365(1–2):52–58. doi: [10.1016/j.memsci.2010.08.033](https://doi.org/10.1016/j.memsci.2010.08.033).
- Feroz H, Bai M, Kwon H, et al. Can fibrous mats outperform current ultrafiltration and microfiltration membranes? *Ind Eng Chem Res*. 2017;56(37):10438–10447. doi: [10.1021/acs.iecr.7b01351](https://doi.org/10.1021/acs.iecr.7b01351).
- Yang C, Topuz F, Park SH, et al. Biobased thin-film composite membranes comprising priamine-genipin selective layer on nanofibrous biodegradable polylactic acid support for oil and solvent-resistant nanofiltration. *Green Chem*. 2022;24(13):5291–5303. doi: [10.1039/D2GC01476A](https://doi.org/10.1039/D2GC01476A).
- Obaid M, Abdelkareem MA, Kook S, et al. Breakthroughs in the fabrication of electrospun-nanofiber-supported thin film composite/nanocomposite membranes for the forward osmosis process: a review. *Crit Rev Environ Sci Technol*. 2020;50(17): 1727–1795. doi: [10.1080/10643389.2019.1672510](https://doi.org/10.1080/10643389.2019.1672510).
- Afsari M, Li Q, Karbassiyazdi E, et al. Electrospun nanofiber composite membranes for geothermal brine treatment with lithium enrichment via membrane distillation. *Chemosphere*. 2023;318:137902. doi: [10.1016/j.chemosphere.2023.137902](https://doi.org/10.1016/j.chemosphere.2023.137902).
- Meng Z, Zhu L, Wang X, et al. Electrospun nanofibrous composite membranes for separations. *Acc Mater Res*. 2023;4(2):180–192. doi: [10.1021/accountsmr.2c00219](https://doi.org/10.1021/accountsmr.2c00219).
- Dadol GC, Kilic A, Tijing LD, et al. Solution blow spinning (SBS) and SBS-spun nanofibers: materials, methods, and applications. *Mater Today Commun*. 2020;25:101656. doi: [10.1016/j.mtcomm.2020.101656](https://doi.org/10.1016/j.mtcomm.2020.101656).
- Liu Y, Zhang G, Zhuang X, et al. Solution blown nylon 6 nanofibrous membrane as scaffold for nanofiltration. *Polymers*. 2019;11(2):1–15. doi: [10.3390/POLYM11020364](https://doi.org/10.3390/POLYM11020364).
- Dadol GC, Lim KJA, Cabatingan LK, et al. Solution blow spinning-polyacrylonitrile-assisted cellulose acetate nanofiber membrane. *Nanotechnology*. 2020; 31(34):345602. doi: [10.1088/1361-6528/ab90b4](https://doi.org/10.1088/1361-6528/ab90b4).
- Ghosh AK, Jeong BH, Huang X, et al. Impacts of reaction and curing conditions on polyamide composite reverse osmosis membrane properties. *J Membr Sci*. 2008;311(1–2):34–45. doi: [10.1016/j.memsci.2007.11.038](https://doi.org/10.1016/j.memsci.2007.11.038).
- Rachamontree P, Sriariyanun M, Tapaamorndech S, et al. Optimization of oil production from cassava pulp and sugarcane bagasse using oleaginous yeast. *Orient J Chem*. 2019;35(2):668–677. doi: [10.13005/ojc/350222](https://doi.org/10.13005/ojc/350222).

21. Chi C, Min Chang H, Li Z, et al. A method for rapid determination of sugars in lignocellulose prehydrolyzate. *BioResources*. 2012;8(1):172–181. doi: [10.15376/biores.8.1.172-181](#).
22. Spiegler KS, Kedem O. Thermodynamics of hyperfiltration (reverse osmosis): criteria for efficient membranes. *Desalination*. 1966;1(4):311–326. doi: [10.1016/S0011-9164\(00\)80018-1](#).
23. Ichi Nakao S, Kimura S. Models of membrane transport phenomena and their applications for ultrafiltration data. *J Chem Eng Jpn*. 1982;15(3):200–205. doi: [10.1252/jcej.15.200](#).
24. Wang X, Ma H, Chu B, et al. Thin-film nanofibrous composite reverse osmosis membranes for desalination. *Desalination*. 2017;420:91–98. doi: [10.1016/j.desal.2017.06.029](#).
25. Yoon K, Hsiao BS, Chu B. High flux nanofiltration membranes based on interfacially polymerized polyamide barrier layer on polyacrylonitrile nanofibrous scaffolds. *J Membr Sci*. 2009;326(2):484–492. doi: [10.1016/j.memsci.2008.10.023](#).
26. Yang Y, Li X, Shen L, et al. A durable thin-film nanofibrous composite nanofiltration membrane prepared by interfacial polymerization on a double-layer nanofibrous scaffold. *RSC Adv*. 2017;7(29):18001–18013. doi: [10.1039/C7RA00621G](#).
27. Ma H, Burger C, Hsiao BS, et al. Ultrafine polysaccharide nanofibrous membranes for water purification. *Biomacromolecules*. 2011;12(4):970–976. doi: [10.1021/bm1013316](#).
28. GC, Dias TS, P, Cellet MC, Santos, et al. PVDF nanofibers obtained by solution blow spinning with use of a commercial airbrush. *J Polym Res*. 2019;26(4):87. doi: [10.1007/s10965-019-1731-7](#).
29. Ma H, Burger C, Chu B, et al. Electrospun nanofibers for environmental protection. In: Hu J, Kumar B, Lu J, editors. *Handbook of fibrous materials*. Weinheim, Germany: Wiley-VCH Verlag GmbH & Co. KGaA; 2020. p. 773–806. doi: [10.1002/9783527342587.ch28](#).
30. Zhuang X, Shi L, Jia K, et al. Solution blown nanofibrous membrane for microfiltration. *J Membr Sci*. 2013;429:66–70. doi: [10.1016/j.memsci.2012.11.036](#).
31. Wang J, Jáklí A, West JL. Airbrush formation of liquid crystal/polymer fibers. *ChemPhysChem*. 2015;16(9):1839–1841. doi: [10.1002/cphc.201500096](#).
32. Sinha-Ray S, Sinha-Ray S, Yarin AL, et al. Theoretical and experimental investigation of physical mechanisms responsible for polymer nanofiber formation in solution blowing. *Polymer*. 2015;56:452–463. doi: [10.1016/j.polymer.2014.11.019](#).
33. Kaur S, Sundarrajan S, Rana D, et al. Influence of electrospun fiber size on the separation efficiency of thin film nanofiltration composite membrane. *J Membr Sci*. 2012;392–393:101–111. doi: [10.1016/j.memsci.2011.12.005](#).
34. Modi R, Mehta R, Brahmbhatt H, et al. Tailor made thin film composite membranes: potentiality towards removal of hydroquinone from water. *J Polym Environ*. 2017;25(4):1140–1146. doi: [10.1007/s10924-016-0887-z](#).
35. De Guzman MR, Ang MBMY, Huang SH, et al. Optimal performance of thin-film composite nanofiltration-like forward osmosis membranes set off by changing the chemical structure of diamine reacted with trimesoyl chloride through interfacial polymerization. *Polymers*. 2021;13(4):544. doi: [10.3390/polym13040544](#).
36. Souza MA, Sakamoto KY, Mattoso LHC. Release of the diclofenac sodium by nanofibers of poly(3-hydroxybutyrate-co-3-hydroxyvalerate) obtained from electrospinning and solution blow spinning. *J Nanomater*. 2014;2014(1):1–8. doi: [10.1155/2014/129035](#).
37. Khorshidi B, Thundat T, Fleck BA, et al. A novel approach toward fabrication of high performance thin film composite polyamide membranes. *Sci Rep*. 2016;6(1):22069. doi: [10.1038/srep22069](#).
38. Dalwani M, Benes NE, Bargeman G, et al. Effect of pH on the performance of polyamide/polyacrylonitrile based thin film composite membranes. *J Membr Sci*. 2011;372(1-2):228–238. doi: [10.1016/j.memsci.2011.02.012](#).
39. Brás T, Guerra V, Torrado I, et al. Detoxification of hemicellulosic hydrolysates from extracted olive pomace by diananofiltration. *Process Biochem*. 2014;49(1):173–180. doi: [10.1016/j.procbio.2013.09.017](#).
40. Maiti SK, Lukka Thuyavan Y, Singh S, et al. Modeling of the separation of inhibitory components from pretreated rice straw hydrolysate by nanofiltration membranes. *Bioresour Technol*. 2012;114:419–427. doi: [10.1016/j.biortech.2012.03.029](#).
41. Weng YH, Wei HJ, Tsai TY, et al. Separation of furans and carboxylic acids from sugars in dilute acid rice straw hydrolyzates by nanofiltration. *Bioresour Technol*. 2010;101(13):4889–4894. doi: [10.1016/j.biortech.2009.11.090](#).
42. Jiang K, Kuang H, Qin T, et al. Recovery of monosaccharides from dilute acid corncob hydrolysate by nanofiltration: modeling and optimization. *RSC Adv*. 2018;8(23):12672–12683. doi: [10.1039/c8ra00236c](#).
43. Ma H, Burger C, Hsiao BS, et al. Highly permeable polymer membranes containing directed channels for water purification. *ACS Macro Lett*. 2012;1(6):723–726. doi: [10.1021/mz300163h](#).
44. Bannani Y, Kosutić K, Drazević E, et al. Wastewater from wood and pulp industry treated by combination of coagulation, adsorption on modified clinoptilolite tuff and membrane processes. *Environ Technol*. 2012;33(10-12):1159–1166. doi: [10.1080/09593330.2011.610828](#).
45. Nghiem LD, Hawkes S. Effects of membrane fouling on the nanofiltration of pharmaceutically active compounds (PhACs): mechanisms and role of membrane pore size. *Sep Purif Technol*. 2007;57(1):176–184. doi: [10.1016/j.seppur.2007.04.002](#).
46. Farahbakhsh J, Vatanpour V, Khoshnam M, et al. Recent advancements in the application of new monomers and membrane modification techniques for the fabrication of thin film composite membranes: a review. *React Funct Polym*. 2021;166:105015. doi: [10.1016/j.reactfunctpolym.2021.105015](#).
47. Zhou F, Wang C, Wei J. Separation of acetic acid from monosaccharides by NF and RO membranes: performance comparison. *J Membr Sci*. 2013;429:243–251. doi: [10.1016/j.memsci.2012.11.043](#).
48. Kim JH, Na JG, Yang JW, et al. Separation of galactose, 5-hydroxymethylfurfural and levulinic acid in acid hydrolysate of agarose by nanofiltration and electrodialysis. *Bioresour Technol*. 2013;140:64–72. doi: [10.1016/j.biortech.2013.04.068](#).
49. Weng YH, Wei HJ, Tsai TY, et al. Separation of acetic acid from xylose by nanofiltration. *Sep Purif Technol*. 2009;67(1):95–102. doi: [10.1016/j.seppur.2009.03.030](#).

50. Ernst M, Bismarck A, Springer J, et al. Zeta-potential and rejection rates of a polyethersulfone nanofiltration membrane in single salt solutions. *J Membr Sci.* 2000; 165(2):251–259. doi: [10.1016/S0376-7388\(99\)00238-0](https://doi.org/10.1016/S0376-7388(99)00238-0).
51. Hagemeyer G, Gimbel R. Modelling the salt rejection of nanofiltration membranes for ternary ion mixtures and for single salts at different pH values. *Desalination.* 1998; 117(1-3):247–256. doi: [10.1016/S0011-9164\(98\)00109-X](https://doi.org/10.1016/S0011-9164(98)00109-X).
52. dos Santos JLC, Fernandes MC, Lourenço PML, et al. Removal of inhibitory compounds from olive stone auto-hydrolysis liquors by nanofiltration. *Desalin Water Treat.* 2011;27(1-3):90–96. doi: [10.5004/dwt.2011.2063](https://doi.org/10.5004/dwt.2011.2063).
53. Luo J, Wan Y. Effects of pH and salt on nanofiltration-a critical review. *J Membr Sci.* 2013;438:18–28. doi: [10.1016/j.memsci.2013.03.029](https://doi.org/10.1016/j.memsci.2013.03.029).